Research on Chemical Intermediates (2025) 51:367–384
https://doi.org/10.1007/s11164-024-05450-y

Sonocatalytic performance of CuO/WO_3 nanoparticles for degradation of methylene blue

Hafize Nagehan Koysuren[1] · **Ozcan Koysuren**[2]

Received: 4 September 2024 / Accepted: 11 November 2024 / Published online: 17 November 2024

Abstract

CuO, WO_3 and CuO/WO_3 composite catalysts were synthesized by using a sol–gel technique. The as-prepared catalyst nanoparticles were characterized by using FTIR, XRD, FESEM, fluorescence spectroscopy and UV–Vis absorbance spectroscopy. FTIR and XRD analyzes showed that CuO and WO_3 nanoparticles were successfully synthesized. FESEM images revealed homogeneous distribution of composite components within each other. The optical band gap of WO_3 was narrowed with the inclusion of CuO. The sonocatalytic activity of the as-prepared samples was studied by sonocatalytic degradation of an organic dye, methylene blue, under ultrasonic irradiation. The effect of catalyst loading and radical scavenger on the dye degradation rate was also examined. All composite samples exhibited higher sonocatalytic activity than pure samples. The highest sonocatalytic dye degradation efficiency (52.7%) was obtained with the CuO/WO_3 composite at a 2/1 mol ratio. After five cycle experiments, the sonocatalytic dye degradation efficiency of the CuO/WO_3 composite decreased slightly to 36.7%.

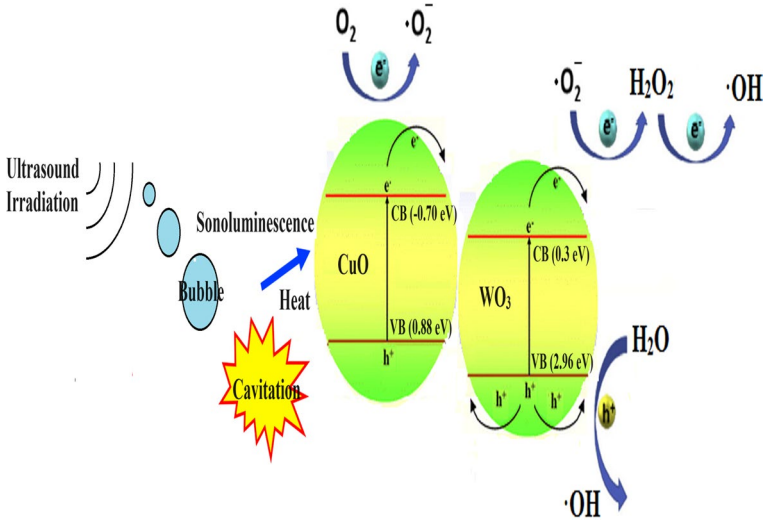

Extended author information available on the last page of the article

Keywords Sonocatalytic · Decolorization · CuO · WO_3 · Methylene blue

Introduction

Organic dyes threaten human health by causing environmental pollution [1]. One of the most used organic dyes, which is environmentally persistent, carcinogenic, toxic and mutagenic, is methylene blue [2]. Methylene blue is widely used as synthetic dye in the textile, cosmetics and leather industries [1, 2]. Depending on the extent of industrial use, large amounts of methylene blue dye containing wastewater are discharged into groundwater and surface water. The monoamine oxidate inhibitory properties of methylene blue pose a threat to fauna in the aquatic ecosystem and may cause fatal serotonin toxicity in humans [2]. Also, methylene blue can cause fever, pain, chest, nausea and hypotension in humans. On the other hand, by covering plant surfaces, it can reduce the amount of light absorbed by plants, which is necessary for photosynthesis [3]. In addition, methylene blue can remain intact in the physical environment for a long time due to its non-biodegradable feature and due to its resistance to environmental conditions such as temperature and light. Therefore, it is extremely important and mandatory to remove methylene blue from wastewaters [2]. In addition, it is necessary and important to develop a green and valuable technology for the removal of methylene blue from wastewaters. Advanced oxidation processes are among the most effective wastewater treatment methods. With the advanced oxidation processes, all kinds of organic pollutants can be converted into harmless products using reactive oxygen species such as superoxide ($\cdot O_2^-$) and hydroxyl (·OH) radicals [1]. Advanced oxidation processes are divided into four different types as chemistry, photochemistry, electrochemistry and sonochemistry based on the reactive species production techniques [4]. Among the advanced oxidation processes, sonolysis has attracted great attention owing to its environmental friendliness, simplicity and wide application range [1, 3]. The sonolysis is based on the cavitation effect produced in an ultrasonic field. Sonication in an aqueous environment gives rise to the rapid formation, growth and violent collapse of cavitation bubbles [5]. The cavitation effect can form local hot spots at around 4000 K and over 1000 atm, which can decompose water molecules into hydroxyl (·OH) and hydrogen (·H) radicals with a high oxidative potential [6, 7]. The resulting radicals can also react with each other to generate hydrogen peroxide (H_2O_2) and hydrogen (H_2). All radicals are responsible for the ultrasound-assisted sonochemical reactions [7]. The cavitation effect can also generate sonoluminescence, which leads to form electron–hole pairs on a semiconductor catalyst [6]. Especially, the hydroxyl radicals have stronger oxidation power than other oxidants and can decompose the organic compounds, including methylene blue, into small harmless molecules such as H_2O and CO_2 [3, 5]. But the sonolysis alone is a time-consuming and energy-wasting process and exhibits low degradation efficiency towards persistent organic pollutants [3]. Some semiconductor materials have the effect of photo-thermal catalysis and heterogeneous nucleation. Additionally, they can take advantage of the heat and sonoluminescence produced by the cavitation effect. Hence, sonocatalytic activity,

which is the combination of the semiconductor catalyst and the sonolysis, is widely used in the removal of organic pollutants from wastewater [3]. Nowadays, various semiconductors such as TiO_2 [8], MoS_2 [9], ZnO [10], $Ce_2Sn_2O_7$ [11], $NiTiO_3$ [12], CuO [13], Cu_2ZnSnS_4 [14], $SbVO_4$ [15] and FeNbO [16] have been applied as sonocatalysts in order to increase the performance of sonolysis in removing organic pollutants from wastewater.

Copper oxide (CuO), which is a p-type semiconductor, has unique properties such as easy synthesis, low cost, non-toxicity, chemical and physical stability. Also, it has a narrow optical band gap. It has been used in several applications such as catalysts, gas sensors and personal care products. CuO nanoparticles have been preferred in many studies in the field of the sonocatalysis due to their higher sonocatalytic efficiency with a large surface/volume ratio [17]. CuO can effectively generate sonoluminescence derived electron–hole pairs [18]. However, in practice, it cannot be used alone because of the high recombination rate of its mobile charge carriers [17]. In addition, CuO exhibits poor charge carrier mobility [18]. To suppress the recombination of the sonoluminescence induced mobile charge carriers, CuO needs to be combined with another semiconductor material in a heterojunction structure [17]. In the literature to overcome the specified problem, CuO was combined with hydrochar [19], TiO_2 [20], Fe_3O_4-ZnO [21] and Fe_3O_4-Mn_3O_4 [22], respectively.

Khataee and his co-workers (2021) achieved a sonocatalytic dye degradation value of almost 86% after 90 min of sonication with Cu_2O–CuO/hydrochar composite catalyst [19]. In another study, Taufik and his co-workers (2018) studied sonophotocatalytic activity of CuO/TiO_2 system. Compared to pure TiO_2 and CuO, there was at least a 1.5-fold increase in the sonophotocatalytic dye degradation rate with the CuO/TiO_2 composite catalyst. The CuO/TiO_2 composite catalyst had a well-matched band edge, providing the formation of a *n–p* junction. The n-p type heterojunction structure promoted charge carrier transfer between the composite components and inhibited the recombination of both sonoinduced and photoinduced electron–hole pairs on the catalyst structure [20]. Within this scope, Taufik and Saleh (2017) studied the sonocatalytic activity of Fe_3O_4/ZnO/CuO system and obtained almost 60% dye degradation after 120 min of sonication [21]. According to the sonocatalytic dye degradation results, it can be concluded that the heterojunction composite structure was successful in increasing the sonocatalytic activity of CuO.

As a narrow-band gap semiconductor catalyst, the combination of CuO with a semiconductor material with a wider band gap might enhance the sonocatalytic activity compared to pure CuO. Among various semiconductor catalyst, tungsten(VI) oxide (WO_3), with a band gap energy of 2.8 eV, has attracted great attention owing to its high oxidative feature, stability, non-toxicity and cost-effectiveness [23]. In addition, WO_3 has been recognized as a promising material for many optical and electronic applications such as supercapacitors, batteries, catalysis, photodiodes, solar cells and gas sensors [7, 23]. WO_3 could be combined with CuO in the composite structure to enhance the visible light absorption and suppress the recombination of the sonogenerated electron–hole pairs on CuO.

Hunge and his coworkers (2018) reported the effect of the incorporation of ZnO nanoparticles in WO_3. WO_3-ZnO nanocomposites exhibits enhanced sonocatalytic activity (~90%) as compared to pure WO_3 sonocatalyst (~60%) in 40 min [7]. In

another study, Khataee and his coworker (2020) reported a study on a Z-scheme WO_3/CoFe-LDH nanocomposite. The sonocatalytic dye degradation ratio of WO_3 (~ 50%) was enhanced to almost 65% with the composite under ozone gas after 30 min of sonication [24]. In an alternative study, $AgFeO_2/WO_3$ was used as a sonocatalyst for the removal of organic pollutants. Over 90% sonocatalytic organic dye removal was achieved with the composite within 35 min. Approximately 80% improvement in sonocatalytic activity was achieved compared to pure WO_3 [23]. Within this scope, Li and his coworkers (2023) fabricated $K_3PMo_{12}O_{40}/WO_3$ crystals via a facile solution method. Almost all the model dye was decomposed within 120 min under ultrasonic irradiation [25].

In the present study, it was attempted to prepare CuO/WO_3 composites by a sol–gel process. The sonocatalytic activity of the CuO/WO_3 composites was studied for the degradation of a model dye (methylene blue) under ultrasonic irradiation. The objective of the study was to evaluate the application potential of the CuO/WO_3 composite in the removal of organic pollutants from wastewater. No reports are available in the literature on the sonocatalytic degradation of methylene blue using the CuO/WO_3 composite, which is novelty of the present study. While high-power ultrasonic probes have been preferred in the removal of pollution from the wastewater by the sonocatalytic degradation method in the literature, in this study, the dye degradation experiment was carried out under ultrasonic vibration applied by a low-power ultrasonic bath. Low-power wastewater treatment systems are important in terms of the applicability of the conducting studies in the industrial field. It also reveals the novelty of the present study.

Experimental

Synthesis of WO_3, CuO and CuO/WO_3 composites

Pure WO_3 nanoparticles were synthesized using a co-precipitation technique [26]. Dissolving of 3 g of sodium tungstate dihydrate ($Na_2WO_4{\cdot}2H_2O$, Sigma-Aldrich) in 20 ml of distilled water was the first step. The resulting solution was subjected to 30 min of magnetic stirring. The as-prepared solution was supplemented with 20 ml of hydrochloric acid (HCl, 8 M, Sigma-Aldrich), and the resulting solution was kept stirring for 2 h at 80 °C. Then the aforementioned solution was left to cool. Following the completion of cooling to room temperature, WO_3 as a yellow precipitate was obtained. The as-prepared WO_3 nanoparticles were isolated form the solution using vacuum filtration, and then rinsed with distilled water. After that the WO_3 nanoparticles were dried in an oven at 60 °C for 12 h, and heat treated in a furnace at 600 °C for 3 h [26].

The solution combustion technique was followed to synthesize pure CuO nanoparticles [27]. The stoichiometric ratio of copper (II) nitrate trihydrate ($CuO(NO_3)_2{\cdot}3H_2O$, Merck) and citric acid ($C_6H_8O_7{\cdot}H_2O$, Merck) were dissolved in 30 ml of distilled water. Copper (II) nitrate trihydrate and citric acid were used

as oxidizer and fuel, respectively. Then the as-prepared solution was magnetically stirred on a preheated plate at 100℃. The aforementioned solution was continued to stir at 100 °C for several hours until the solution became a viscous gel. Once the solution became a viscous gel, it began a self-sustaining combustion reaction. Afterward, CuO in powder form was obtained. Finally, the as-prepared CuO powder was ground to fine powder, and heat treated at 300 °C for 3 h [27]. With the inclusion of WO_3 nanoparticles, the synthesis of pure CuO was also carried out in a similar method to obtain CuO/WO_3 composites. The composite samples were labeled as CuO/WO_3(1/2), CuO/WO_3(1/1) and CuO/WO_3(2/1) based on the molar ratio of CuO–WO_3.

Methods of characterization

The X-ray diffraction technique (Inel Equinox 1000) was used with CoKα radiation in the range of 20° to 70° to obtain the X-ray diffraction (XRD) patterns of the prepared samples. The Fourier transform infrared (FTIR) spectrum with Perkin Elmer 400 model spectrophotometer was employed to detect the presence of functional groups in the prepared samples. The morphology of the prepared samples was investigated using field emission scanning electron microscopy (Quanta 400 F). To study the optical properties, UV–Vis absorbance spectrum of the prepared samples was recorded using a UV–Vis spectrophotometer (Genesys 10S, Thermo Scientific). The fluorescence spectrum of the prepared samples was recorded on a Lumina model fluorescence spectrophotometer (Thermo Scientific).

The sonocatalytic activity of the prepared samples was studied by degrading the model dye, methylene blue. Initial concentration of the dye solution was fixed to 10 mg/l for all the degradation experiments. The sonocatalyst sample was dispersed in the dye solution to form 1 g/l catalyst suspension. The dye degradation experiment was performed using the as-prepared catalyst suspension under ultrasonic vibration imparted by an ultrasonic bath (40 kHz, 120 W). Before the sonocatalytic degradation experiment, the suspension was stirred for half an hour using a magnetic stirrer to ensure adsorption–desorption equilibrium between the dye molecules and the catalyst sample. On attainment of adsorption–desorption equilibrium, the dye solution was exposed to ultrasonic irradiation. 2 ml of the dye solution was acquired after every 30 min interval of the sonocatalytic degradation experiment. The sonocatalyst nanoparticles were separated from the dye solution by centrifuging. The concentration of methylene blue in the solution was determined using a UV–Vis spectrophotometer (Genesys 10S, Thermo Scientific). The dye degradation ratio was calculated using the following equation:

$$\text{Dye degradation ratio}\% = \left(C_0 - C\right)/C_0 \quad (1)$$

where the symbol C_0 and C were the initial concentration of methylene blue and the concentration of methylene blue after ultrasonic irradiation.

To investigate the sonocatalytic dye degradation mechanism, potassium persulfate (1 mM) as an electron scavenger and ammonium oxalate (1 mM) as a hole scavenger were added into the methylene blue solution. Within the scope of the scavenger test, tert-butanol (6 ml/100 ml dye solution) and ascorbic acid (1 mg/100 ml dye solution), which acted as hydroxyl radical and superoxide radical scavengers, respectively, were added into the methylene blue solution. In addition, the effect of methanol on the sonocatalytic activity was studied. For this purpose, methanol (6 ml/100 ml dye solution) was added into the methylene blue solution. To study the reusability of the prepared sonocatalysts, the catalyst sample was removed from the dye solution using vacuum filtration and rinsed with distilled water. After drying, the catalyst sample was added into the dye solution for the following sonocatalytic degradation cycle. To analyze the synergistic effect of sonocatalytic activity with photocatalytic activity, a 300 W visible light lamp (Osram Ultravitalux) was used. The mineralization ratio of the dye solution exposed to ultrasonic vibration was determined by using a Analytikjena model (multi N/C 2100S direct injection) total organic carbon (TOC) analyzer.

Results and discussion

FTIR analysis

Figure 1 illustrates the FTIR spectrum of pure CuO, pure WO_3 and the CuO/WO_3(2/1) composite. As can be seen from the FTIR spectrum of CuO, there is a sharp absorbance peak at around 475 cm^{-1} and a weak peak at 586 cm^{-1}, which could be attributed to the Cu–O stretching vibration (Fig. 1a). The appearance of a weak absorbance peaks at around 1350 cm^{-1} could be attributed to the –C–O stretching vibration [28]. On the other hand, the FTIR spectrum of WO_3 illustrates an intense absorption band between 984 cm^{-1} and 432 cm^{-1} (Fig. 1b), which could be corresponded to the lattice vibrational modes of WO_3. The sharp peak on the mentioned absorbance band at 802 cm^{-1} could be assigned to the O–W–O stretching vibration. In addition, there is a weak absorbance band at around 3430 cm^{-1}, could be attributed to the vibrations of the distorted water molecules [29]. Moreover, the FTIR spectrum of the CuO/WO_3(2/1) composite shows absorbance peaks at wavenumbers similar to those of CuO and WO_3, which indicated the presence of both CuO and WO_3 in the composite structure. The peak of the Cu–O bond was observed at 472 cm^{-1}, and the peak of the O–W–O bond was observed at 800 cm^{-1} (Fig. 1c) [28, 29]. Figure S1 exhibits the FTIR spectrum of the five times of recycled CuO/WO_3(2/1). For the five times of recycled CuO/WO_3(2/1), the characteristic absorbance peaks of CuO and WO_3 appeared in the same wavelength range between 1000–400 cm^{-1} (Fig. S1). No additional absorbance peak was observed in the FTIR spectrum of the five-times recycled CuO/WO_3(2/1), suggesting that no significant chemical change occurred in the CuO/WO_3(2/1) catalyst. According to the FTIR analysis, the CuO/WO_3(2/1) catalyst preserved its chemical structure, which made it a suitable catalyst for repeated use.

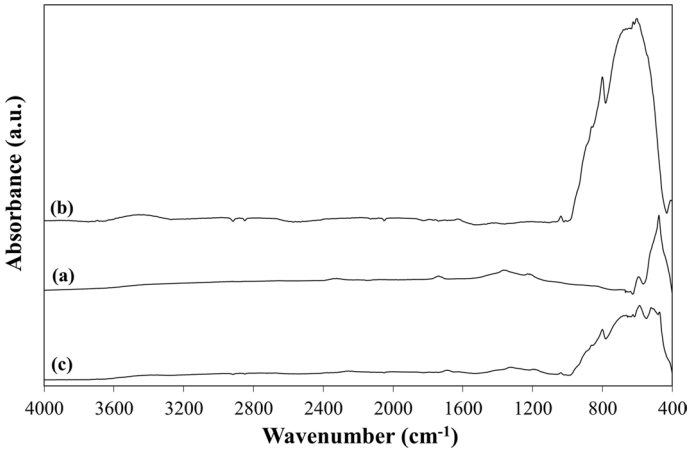

Fig. 1 FTIR spectrum of **a** CuO, **b** WO_3 and **c** $CuO/WO_3(2/1)$

XRD analysis

The X-ray diffraction pattern of pure CuO, pure WO_3 and the $CuO/WO_3(2/1)$ composite is illustrated in Fig. 2. From the XRD pattern it was observed that all the samples were polycrystalline in nature. Pure CuO displayed the diffraction peaks at 37.2°, 40.6°, 44.3°, 50.7°, 56.2°, 61.7° and 67.5°, which were assigned to the (−111), (200), (−112), (−202), (202), (−113) and (−311) crystal planes, respectively (Fig. 2a) [30]. Most of the diffraction peaks presented in the XRD pattern of pure WO_3 were completely matched to the diffraction peaks of the standard sample (JCPDS 20–1324). The diffraction peaks of WO_3 were observed at $2\theta = 23.1°$, 23.6°, 24.4°, 26.6°, 28.7°, 33.3°, 34.2°, 35.6°, 41.9°, 47.2°, 48.3°, 49.9°, 55.9°, 59.4° and 62.4°, denoting diffractions from the (002), (020), (200), (120), (112), (022), (202), (−122), (222), (004), (040), (140), (420), (242) and (340) crystalline surfaces, respectively (Fig. 2b) [31]. According to Fig. 2c, all the above-mentioned diffraction peaks for pure CuO and WO_3 were observed in the XRD diffractogram of the $CuO/WO_3(2/1)$ composite, which implied the successful synthesis of the $CuO/WO_3(2/1)$ composite. The XRD diffractogram of the composite sample revealed that the diffraction peaks related to both CuO and WO_3 exhibited minor changes in the diffraction angle, revealing the strong interaction between the composite constituents. Additionally, the change in peak intensities observed in the composite sample revealed minor changes in the arrangement of the CuO crystal structure with the addition of WO_3 [24].

Morphological analysis

FESEM analyses of pure CuO, pure WO_3 and the composite samples were performed to reveal the surface morphology (Fig. 3). FESEM image of pure CuO illustrates spherical structures of CuO in an aggregate form. Homogeneous structures of

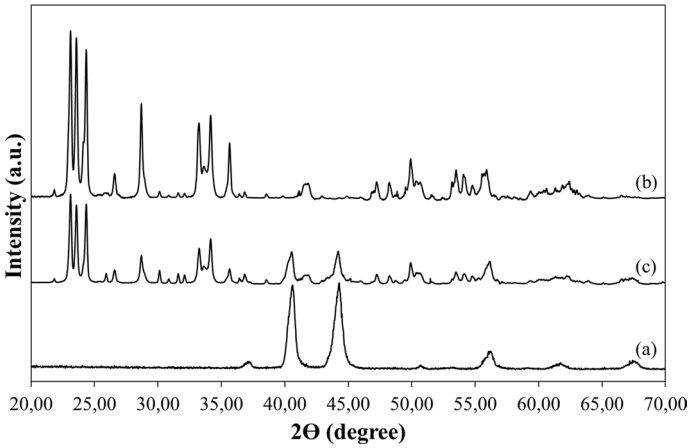

Fig. 2 XRD pattern of **a** CuO, **b** WO_3 and **c** CuO/WO_3(2/1)

approximately the same shape and size with an average diameter of approximately 100 nm were obtained (Fig. 3a). According to FESEM images (Fig. 3b-3c), spherical structures of CuO nanocrystals were grown on the WO_3 nanoparticles. The as-synthesized CuO nanoparticles were uniformly dispersed on the WO_3 phase. The interfacial contact and interaction between the CuO and WO_3 nanoparticles appeared to be good. Homogeneous distribution of nanoparticles within each other was observed. FESEM image of pure WO_3 shows non-uniform sphere-like nanoparticles with an average diameter of about 300 nm. It was understood that the WO_3 nanoparticles also tended to agglomerate (Fig. 3d).

UV–Vis absorption spectroscopy

The UV–Vis absorbance spectrum was used to study the optical absorption properties of the samples (Fig. 4). The UV–Vis spectrum of pure CuO illustrates a broad absorption band between 200–500 nm from the UV light region to the visible light region (Fig. 4a). The UV–Vis absorbance spectrum of pure WO_3 shows a stronger and narrower absorption band between 200 and 350 nm in the UV light region (Fig. 4b). According to Fig. 4c–e, the UV–Vis absorbance spectrum of the CuO/WO_3 composites exhibited a red shift compared to pure WO_3. CuO broadened the optical response of pure WO_3 in the composite structure.

The UV–Vis absorbance spectrum was also used to estimate the optical band gap (Eg) of the samples according to the Tauc's equation:

$$(\alpha h\nu)^2 = A(h\nu - \mathrm{Eg}) \tag{2}$$

where α, hν, and A are the absorption coefficient, the photon energy and the energy-independent coefficient, respectively. The optical band gap was estimated with extrapolation of the plot of $(\alpha h\nu)^2$ vs. hν to the photon energy axis (Fig. 5) [22]. The optical band gap value of pure CuO, WO_3, CuO/WO_3(1/2), CuO/WO_3(1/1), CuO/

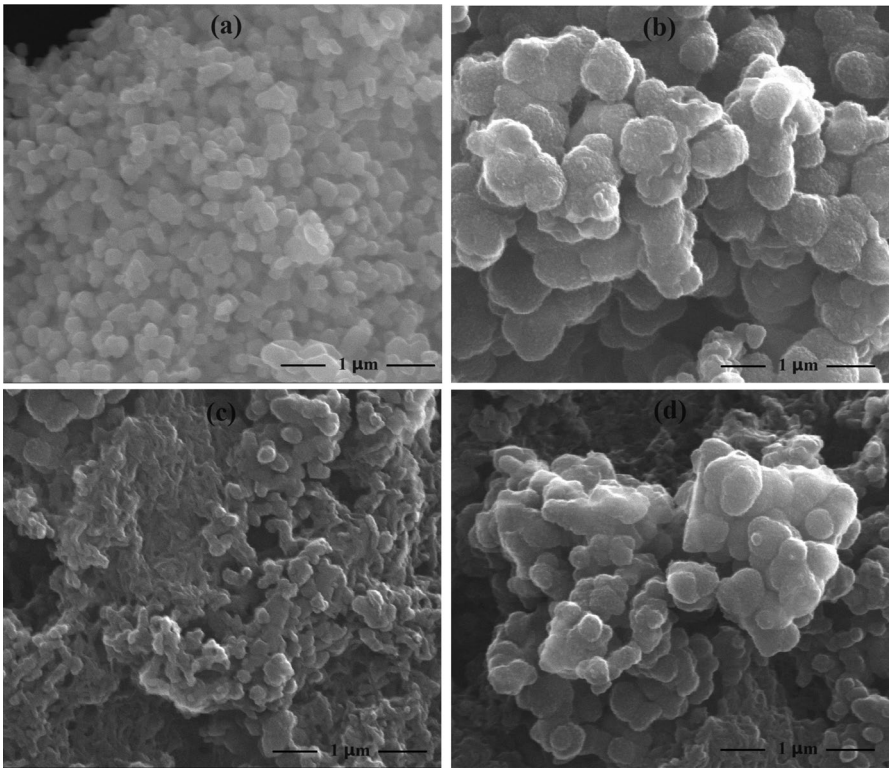

Fig. 3 FESEM image of **a** CuO, **b** CuO/WO_3(1/2), **c** CuO/WO_3(2/1) and **d** WO_3

WO_3(2/1) was found to be 1.1 eV, 2.2 eV, 1.9 eV, 1.8 eV and 1.7 eV, respectively. Compared to pure WO_3, the composites had narrower optical band gap and the estimated band gap value continued to decrease with the increase in the CuO content of the composite. The ultrasonic irradiation-induced sonoluminescence generates a radiation with a wavelength below 420 nm (2.95 eV) [7]. Therefore, all prepared samples had a suitable optical band gap to absorb sonoluminescence light.

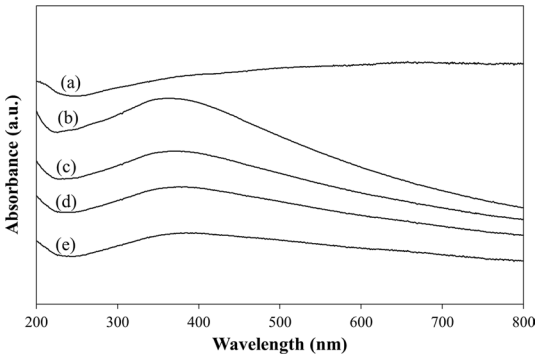

Fig. 4 UV–Vis absorption spectrum of **a** CuO **b** WO_3, **c** CuO/WO_3(1/2), **d** CuO/WO_3(1/1) and **e** CuO/WO_3(2/1)

Fluorescence spectral analysis

To observe the recombination rate of the sonoinduced electron–hole pairs on the prepared samples, the fluorescence spectra were recorded and their results are illustrated in Fig. 6. Any change in the recombination rate of the sonoinduced charge carriers can be demonstrated by comparing the peak intensities of the fluorescence signals. According to Fig. 6, the fluorescence peak intensity of WO_3 at around 630 nm is quite high, meaning that the sonoinduced electrons of WO_3 quickly recombined with the sonoinduced hole in the valence band. On the other hand, the fluorescence peak intensity of CuO was slightly lower than that of WO_3. A significant decrease in the fluorescence peak intensity was observed when CuO was combined with WO_3 in the composite structure. The decrease in the fluorescence peak intensity indicated that the recombination rate of the sonoinduced electron–hole pairs was suppressed at a certain extent.

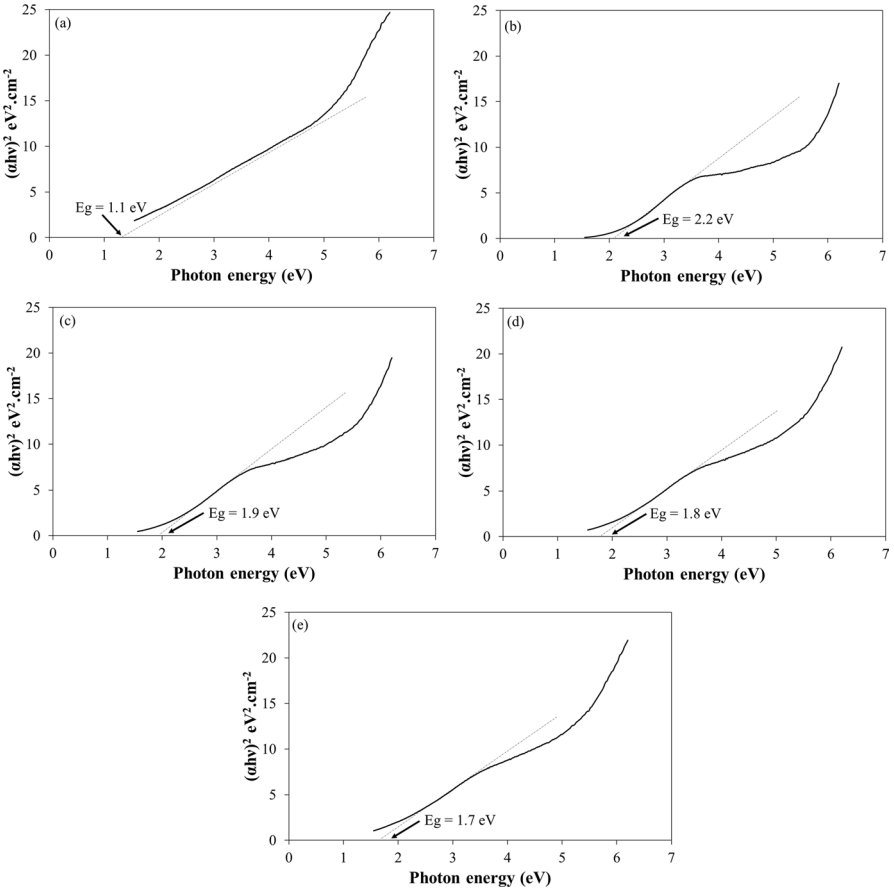

Fig. 5 Tauc's plot for **a** CuO, **b** WO_3, **c** CuO/WO_3(1/2), **d** CuO/WO_3(1/1) and **e** CuO/WO_3(2/1)

Photocatalytic activity

Figure S2 illustrates absorption spectral changes of methylene blue over pure CuO, WO_3 and the CuO/WO_3 composites. Methylene blue over the composite samples exhibited lower absorbance peaks when compared with pure CuO and pure WO_3. The sonocatalytic dye degradation ratios are presented in Fig. 7a. The sonocatalytic dye degradation ratios with pure CuO and pure WO_3 were 28.3% and 27.2%, respectively, after 180 min of sonication. In the presence of the CuO/WO_3(1/2), CuO/WO_3(1/1) and CuO/WO_3(2/1) composites, the sonocatalytic dye degradation ratios were 35.7%, 47.5% and 52.7%, respectively, after 180 min of sonication. All the composite samples exhibited higher sonocatalytic activity than that of pure CuO and pure WO_3. The reported conduction band energy edges of CuO and WO_3 are −0.70 eV and 0.30 eV (vs. NHE), respectively. In addition, the reported valence band energy edges of CuO and WO_3 are 0.88 eV and 2.96 eV (vs. NHE), respectively [32, 33]. Under ultrasonic irradiation-induced sonoluminescence, both CuO and WO_3 might be excited to produce electron–hole pairs. The acoustic cavitation under ultrasonic irradiation was responsible for the sonoluminescence, leading to generate a radiation with a wavelength below 420 nm [7]. According to Fig. 8, the conduction band and valence band edges of CuO were more negative than that of WO_3. Due to the difference between the band potentials of CuO and WO_3 (Fig. 8), combining these two semiconductors in the composite heterojunction structure might cause the sonoinduced holes to move from valence band of WO_3 to the valence band of CuO [32, 33]. Meanwhile, the sonoinduced electrons of CuO might transfer to the conduction band of WO_3. Therefore, the recombination of the sonoinduced electron–hole pairs might be suppressed and the separation of the sonoinduced charge carriers might be accomplished. This might be the reason for the enhancement in the sonocatalytic activity with the CuO/WO_3 composite (Fig. 7a). There are a few studies in the literature on the sonocatalytic degradation of methylene blue using CuO- or WO_3-based composites. But, there is no study on the sonocatalytic dye degradation in the presence of the CuO/WO_3 composite. Therefore, it is not easy to compare the dye degradation data of this study with the literature data. In general, dye degradation values obtained in the presence of CuO-based or WO_3-based composite catalysts in the literature are close to the sonocatalytic dye

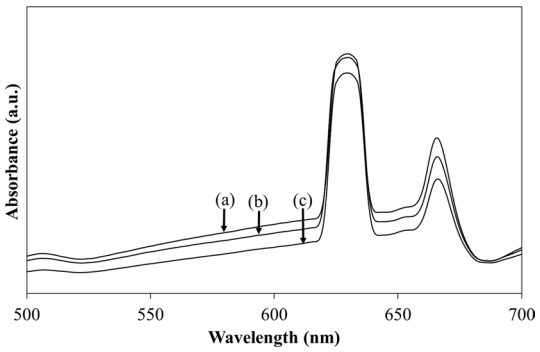

Fig. 6 Fluorescence spectrum of **a** WO_3, **b** CuO and **c** CuO/WO_3(2/1)

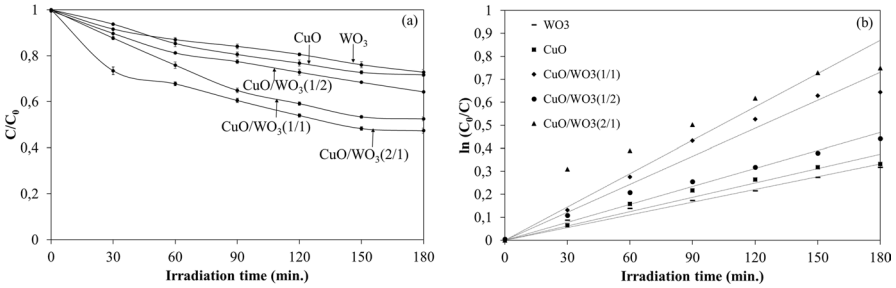

Fig. 7 **a** The sonocatalytic dye degradation ratio in the presence of the prepared samples, **b** The sonocatalytic dye degradation kinetics in the presence of the prepared samples

degradation values of the present study. Unlike other studies, in this study, sonocatalytic dye degradation reactions were carried out using a simple low-power ultrasonic bath. A wastewater treatment method with low power requirements has high potential for industrial application. In this respect, the sonocatalytic dye degradation method applied in this study and the obtained degradation data are valuable.

The complete mineralization of methylene blue in aqueous media can be investigated by measuring the total organic carbon (TOC) content [34]. Total organic carbon (TOC) measurement was also taken on the model dye solution exposed to ultrasonic vibration for 180 min in order to determine whether the model dye molecules underwent complete mineralization to CO_2 and H_2O in the presence of the prepared catalyst samples. The complete mineralization ratios with pure CuO and pure WO_3 were 13.1% and 11.9%, respectively, after 180 min of sonication. In the presence of the CuO/WO_3(2/1) composite, the complete mineralization ratio was 34.7% after 180 min of sonication. The CuO/WO_3(2/1) composite sample exhibited higher mineralization ratio than that of pure CuO and pure WO_3. The reason for the enhanced mineralization ratio might be the ability of the CuO/WO_3(2/1) composite to produce reactive oxygen species, which could decompose organic compounds. On the other hand, the complete mineralization ratio at the end of the sonocatalytic degradation reaction was found to be less compared to the sonocatalytic dye degradation ratio, which was evident due to the fact that all the dye molecules were not completely mineralized and were converted into some other components.

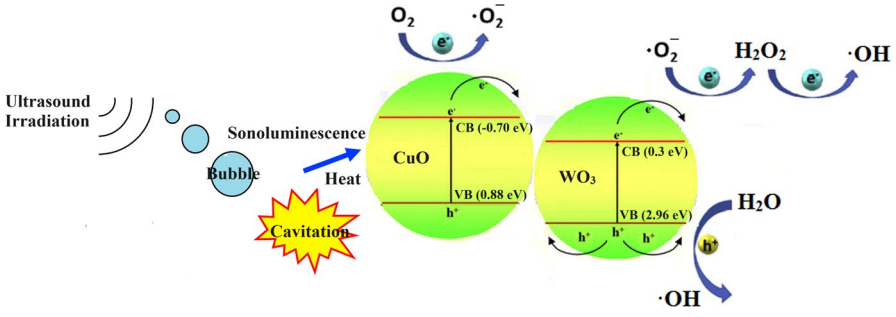

Fig. 8 The proposed sonocatalytic dye degradation mechanism on CuO/WO_3

The possible mechanism of methylene blue degradation on the composite sample is proposed in Fig. 8. The standard potential for water to be oxidized to form hydroxyl radicals (·OH/H_2O) was 2.29 eV vs. NHE [3]. The valence band edge of WO_3 was more positive than the oxidation potential of H_2O to form hydroxyl radicals. In addition, the standard reduction potential of O_2 to form superoxide radicals (O_2/·O_2^-) was −0.33 eV versus NHE [3]. Hence, surface adsorbed O_2 could be reduced to ·O_2^- by the conduction band electrons of CuO. The conduction band edge of WO_3 was not enough negative to reduce O_2 to ·O_2^-. In addition, the valence band edge of CuO was not enough positive to oxidize surface adsorbed water molecules to hydroxyl radicals. According to the redox potentials of H_2O_2/·O_2^- and ·OH/H_2O_2, which are 0.69 eV and 0.38 eV versus NHE, respectively, the conduction band electrons of both CuO and WO_3 could be used to convert superoxide radicals into hydroxyl radicals [35]. The strong oxidability of both hydroxyl and superoxide radicals might lead to decomposition of methylene blue [3]. The radical scavenger experiments also confirmed the activity of both radicals in the sonocatalytic degradation of methylene blue.

The kinetic study of sonocatalytic degradation of methylene blue in the presence of pure CuO, pure WO_3 and the CuO/WO_3 composites was studied using the pseudo-first-order kinetic model as represented by following equation:

$$\ln\left(C_0/C\right) = \mathrm{kt} \tag{3}$$

where C_0 and C were methylene blue concentration before and after sonication, respectively, k is the degradation rate constant and t is the sonication time [14]. The degradation rate constant (k) was estimated from the slope of the ln(C_0/C) versus t plot (Fig. 7b). According to Fig. 7b, the k value of the sonocatalytic dye degradation by pure CuO and WO_3 was estimated to be 0.0021 min^{-1} and 0.0018 min^{-1}, respectively (Table 1). In addition, the k value of methylene blue degradation by the CuO/WO_3(1/2), CuO/WO_3(1/1) and CuO/WO_3(2/1) composites was found to be 0.0026 min^{-1}, 0.0041 min^{-1} and 0.0048 min^{-1}, respectively (Table 1). The reaction rate constant of sonocatalytic dye degradation by the CuO/WO_3(2/1) composite was at least 2 times higher than that of pure CuO and pure WO_3, indicating that combining CuO with WO_3 in the composite structure accelerated the sonocatalytic degradation of methylene blue. The regression coefficient value (R^2) of the sonocatalytic dye degradation reactions was more than 0.86 (Table 1), which indicated that the sonocatalytic dye degradation reactions followed the pseudo-first-order kinetics [36].

The effect of the catalyst loading on the sonocatalytic degradation of methylene blue was investigated and its results are shown in Fig. 9a. According to Fig. 9a, the degradation ratio of methylene blue in the absence of the catalyst was 14.4% after 180 min of sonication. This value increased to 52.7% in the presence of the CuO/WO_3(2/1) composite at 1 g/l loading of CuO/WO_3(2/1). In the presence of semiconductor catalyst nanoparticles, an additional phase is available to enhance the cavitational activity, improving the sonocatalytic activity [37]. In absence of the catalyst, there was only hydroxyl radicals, generated due to the cavitation effect. In the presence of the catalyst, there were also sonogenerated hydroxyl and superoxide radicals, contributing to the degradation of methylene blue. It was observed that the

Table 1 The sonocatalytic dye degradation rate in the presence of the as-prepared samples

Sample	k (min^{-1})	R^2
CuO	0.0021	0.9584
WO_3	0.0018	0.9697
CuO/WO_3(1/2)	0.0026	0.9645
CuO/WO_3(1/1)	0.0041	0.9595
CuO/WO_3(2/1)	0.0048	0.8633

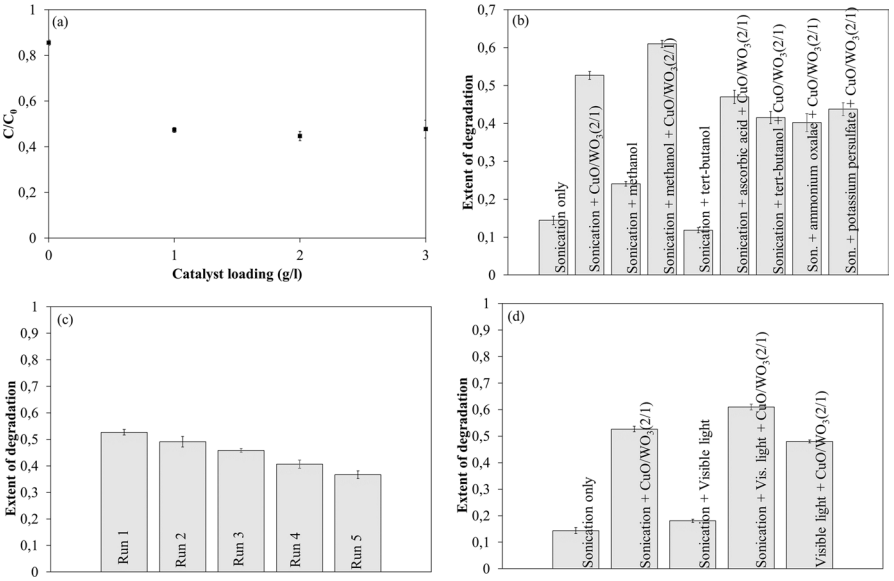

Fig. 9 **a** Effect of the catalyst loading on the sonocatalytic dye degradation efficiency of CuO/WO_3(2/1), **b** Effect of methanol and scavengers (electron–hole and radical) addition on the sonocatalytic dye degradation efficiency, **c** The reusability results of the sonocatalytic dye degradation experiment in the presence of CuO/WO_3(2/1), **d** The synergistic effect of visible light with ultrasonic irradiation on the sonocatalytic dye degradation

degradation ratio of methylene blue fluctuated between 52 and 55% as the amount of the CuO/WO_3(2/1) composite in the dye solution increased. The maximum extent of degradation of methylene blue as 55.3% was observed at a loading of 2 g/l of CuO/WO_3(2/1). According to Fig. 9a, an increase in the catalyst loading beyond 2 g/l of CuO/WO_3(2/1) led to a slight decrease in the dye degradation ratio, which was attributed to the enhanced contribution of scattering effects and attenuation of incident sound energy by the catalyst nanoparticles [37].

The effect of the presence of methanol on the extent of degradation of methylene blue was also studied (Fig. 9b). The degree of degradation of methylene blue in the presence of methanol without the catalyst was 24.1% after 180 min of sonication. The degree of degradation as 60.9% was obtained in the presence of methanol with the CuO/WO_3(2/1) composite after 180 min of sonication.

Methanol addition enhanced both the sonolytic and the sonocatalytic dye degradation ratios. Methanol could form CH_2OH radicals in dye solution. The specified radicals could convert H_2O into hydroxyl radicals, which were necessary for the degradation of organic dye molecules [37]. To reveal the exact role of hydroxyl radicals in the sonolytic and sonocatalytic degradation of the model dye, tert-butanol as a radical scavenger was added into the dye solution with and without the CuO/WO_3(2/1) composite. It was observed that the degree of degradation of methylene decreased from 14.4 to 11.8% in the presence of tert-butanol without the composite catalyst. The degree of dye degradation decreased from 52.7 to 41.5% in the presence of tert-butanol with the CuO/WO_3(2/1) composite after 180 min of sonication (Fig. 9b). The deleterious effect of the presence of tert-butanol could be explained by competitive hydroxyl radical reactions with methylene blue and tert-butanol [37]. To evaluate the exact role of superoxide hydroxyl in the sonocatalytic dye degradation, ascorbic acid as a radical scavenger was added into methylene blue solution with the CuO/WO_3(2/1) composite. The degree of sonocatalytic dye degradation as 47% was obtained in the presence of ascorbic acid with the CuO/WO_3(2/1) composite (Fig. 9b). Both types of the radical scavengers reduced the sonocatalytic dye removal value. The obtained results revealed that both hydroxyl and superoxide radicals played an important role in the sonocatalytic dye degradation reactions. When both radicals were compared, it could be said that the hydroxyl radical was more effective because it reduced the sonocatalytic dye degradation ratio more. The effect of electron and hole scavengers on the sonocatalytic dye degradation ratio of the CuO/WO_3(2/1) catalyst was also studied (Fig. 9b). With the addition of the electron scavenger (potassium persulfate) into the dye solution, the dye degradation ratio decreased from 52.7 to 40.2% at end of 180 min of sonication. Potassium persulfate might consume the sonoinduced electrons in the conduction bands of both CuO and WO_3, which might lead to the specified decrease in the dye degradation ratio. With the addition of the hole scavenger (ammonium oxalate) into the dye solution, the dye degradation ratio decreased from 52.7 to 43.7% at end of 180 min of sonication. It was estimated that due to the consumption of a certain part of the sonoinduced holes by the scavenger, fewer sonoinduced holes remained for the hydroxyl radical generation, leading to a reduction in the sonocatalytic dye degradation efficiency. The electron and hole scavenger experiments revealed that both the sonoinduced electron and the sonoinduced hole were effective in the formation of active radicals to degrade the dye molecules.

Reusability is important for the sustainability of catalysts. The reusability of the CuO/WO_3(2/1) composite was studied by repeated sonocatalytic dye degradation experiments. The dye degradation ratio in the presence of the CuO/WO_3(2/1) decreased from 52.7 to 36.7% after five cycles of sonication (Fig. 9c). The reason for the decrease in the sonocatalytic dye degradation ratio might be the reaction intermediates adhering strongly to the active surface of the composite catalyst. Washing with distilled water might not be sufficient to remove all of the reaction intermediates from the catalyst surface. In general, the prepared composite catalyst exhibited relatively high recyclability. To test the long-term stability of the CuO/WO_3(2/1)

catalyst, the dye degradation ratio after ten cycles of sonication was also examined. The dye degradation ratio decreased to 30.1% within 10 repeated cycles.

Under the synergistic effect of sonolysis and photolysis, only 18.0% methylene blue degradation was achieved without a catalyst under both visible light irradiation and sonication (Fig. 9d). Local hot spots might occur due to the collapse of water bubbles, resulting in local temperature increases. Thermolytic decomposition of H_2O molecules led to form hydroxyl radicals, which could decompose the dye molecules. This phenomenon is called sonolysis [38]. According to Fig. 9d, the sonolysis effect on the dye degradation increased under visible light irradiation, implying that the photolysis had a minor effect on the dye degradation. To reveal the synergistic effect of sonocatalytic activity and photocatalytic activity, the same experiment was performed in the presence of the CuO/WO_3(2/1) composite. The CuO/WO_3(2/1) composite exhibited a dye degradation ratio of 60.9% after 180 min of both sonication and visible light irradiation (Fig. 9d), demonstrating the effectiveness of the photocatalytic activity of the prepared composite. To be sure, the same experiment was performed only under visible light. Approximately 40% of methylene blue was removed from the solution medium in the presence of the CuO/WO_3(2/1) composite after 180 min of visible light irradiation (Fig. 9d).

To reveal the effects of real wastewater medium on the sonocatalytic activity, the sonocatalytic degradation of methylene blue in the real wastewater was also studied. The dye degradation ratio of methylene blue in the real wastewater with the CuO/WO_3(2/1) catalyst was 47.2% in 180 min (Fig. S3). A reduction of approximately 5% in the sonocatalytic dye degradation ratio was recorded when a real wastewater was used instead of distilled water in the preparation of the methylene blue solution. The real wastewater experiment showed that the sonocatalytic activity of the prepared sample slightly affected by the real wastewater environment. Contaminants present in the real wastewater environment might adhere to the catalyst surface, leading to a decrease in the effective catalyst surface [39]. The reduction in the sonocatalytic dye degradation ratio might be attributed to the reduction in the effective surface area of the CuO/WO_3(2/1) sample.

Conclusions

The present study provided a new type of a composite catalyst for the sonocatalytic dye degradation activity. All the prepared samples were successfully synthesized by the sol–gel technique and used for the sonocatalytic degradation of methylene blue in aqueous media. Compared with pure samples, all the composite samples exhibited high sonocatalytic dye degradation performance. The high sonocatalytic activity of the CuO/WO_3 composite was attributed to the synergistic effect between the composite constituents. The initial catalyst loading and methanol addition had a significant effect on the sonocatalytic dye degradation performance. The scavenger experiments revealed that both $\cdot O_2^-$ and ·OH radicals played a major role in the sonocatalytic dye degradation reactions. Visible light irradiation promoted the sonocatalytic dye degradation process, which revealed the synergistic effect of photocatalytic activity with sonocatalytic activity. In conclusion, the CuO/WO_3 composite can

be considered as a promising catalyst for sonocatalytic degradation of organic dyes in wastewater.

Supplementary Information The online version contains supplementary material available at https://doi.org/10.1007/s11164-024-05450-y.

Author contributions O.K. and H.N.K. prepared the main manuscript text. O.K. and H.N.K. draw the figures. Table was prepared also by O.K. and H.N.K.

Funding The authors declare that no funds, grants or other support were received during the preparation of this manuscript.

Data availability No datasets were generated or analyzed during the current study.

Declarations

Conflict of interest The authors declare no competing interests.

References

1. Q. Gao, G. Sun, R. Ling, Y. Cai, A. Wang, J. Mater. Sci-Mater. Electron **33**(34), 25589 (2022)
2. P.O. Oladoye, T.O. Ajiboye, E.O. Omotola, O.J. Oyewola, Results Eng. **1**(16), 100678 (2022)
3. L.L. He, X.Y. Li, J.Y. Bai, S. Li, S. Qi, X. Wang, Y. Li, Surf. Interfaces **31**, 101980 (2022)
4. Y.C. Liu, J.Q. Wang, Y. Wang, C.L. Chen, X. Wang, Z. Xiang, Appl. Catal. A-Gen. **643**, 118776 (2022)
5. P. Amirian, E. Bazrafshan, A. Payandeh, Waste Manage. Res. **35**(6), 636 (2017)
6. Y.L. Pang, A.Z. Abdullah, Ultrason. Sonochem. **19**(3), 642 (2012)
7. Y.M. Hunge, A.A. Yadav, V.L. Mathe, Ultrason. Sonochem. **45**, 116 (2018)
8. S.D. Ayare, P.R. Gogate, Chem. Eng. Process. **154**, 108040 (2020)
9. J. Li, W.B. Ko, Elastom. Compos. **58**(4), 191 (2023)
10. A. Troia, S. Galati, V. Vighetto, V. Cauda, Ultrason. Sonochem. **97**, 106470 (2023)
11. Y. Bie, T. Li, F. Li, Ceram. Int. **49**(14), 22726 (2023)
12. B.P. Long, D. Van Thiet, P.P. Hung, N.H. Tuan, L.H. Bac, Mater. Lett. **356**, 135581 (2024)
13. R. Fekri, S.A. Mirbagheri, E. Fataei, G. Ebrahimzadeh-Rajaei, L. Taghavi, Main Group Chem. **21**(4), 975 (2022)
14. X. Hu, J. Qiao, J. Zhou, J. Bao, W. He, Catal. Lett. **153**(9), 2853 (2023)
15. M. Lü, F. Li, T. Li, J. Non-Cryst, Solids **590**, 121698 (2022)
16. M. He, D. Li, Y. Liu, T. Li, F. Li, J. Fernández-Catalá, W. Cao, New J. Chem. **48**(15), 6704 (2024)
17. K. Ayagh, M. Farrokhi, J.K. Yang, M. Shirzad-Siboni, Environ. Technol. **44**(3), 342 (2023)
18. G. Ebrahimzadeh-Rajaei, Theor. Found. Chem. Eng. **56**(6), 1088 (2022)
19. A. Khataee, D. Kalderis, P.Y. Motlagh, V. Binas, S. Stefa, M. Konsolakis, J. Ind. Eng. Chem. **95**, 73 (2021)
20. A. Taufik, A. Muzakki, R. Saleh, Mater. Res. Bull. **99**, 109 (2018)
21. A. Taufik, R. Saleh, Mater. Sci. Eng. **188**(1), 012005 (2017)
22. M.T. Kaya, M.H. Calimli, N.S. Nas, Res. Chem. Intermed. **49**(6), 2549 (2023)
23. R. Justinabraham, A. Durairaj, S. Vasanthkumar, New J. Chem. **48**(10), 4482 (2024)
24. A. Khataee, A. Fazli, F. Zakeri, S.W. Joo, J. Ind. Eng. Chem. **89**, 301 (2020)
25. L. Li, F. Li, T. Li, W. Cao, RSC Adv. **13**(23), 15981 (2023)
26. T. Thilagavathi, D. Venugopal, R. Marnadu, J. Chandrasekaran, T. Alshahrani, M. Shkir, J. Inorg. Organomet. Polym. Mater. **31**(3), 1217 (2021)
27. S.J. Singh, P. Chinnamuthu, Colloid Surf. A-Physicochem. Eng. Asp. **625**, 126864 (2021)
28. I. Kir, H.A. Mohammed, S.E. Laouini, M. Souhaila, G.G. Hasan, J.A. Abdullah, S. Mokni, A. Naseef, A. Alsalme, A. Barhoum, J. Polym. Environ. **32**(2), 718 (2024)
29. T. Iqbal, R.M. Munir, A. Younas, S. Afsheen, M.S. Mansha, S. Ahsan, A.A. AlObaid, N. Al-Zaqri, J. Inorg. Organomet. Polym. Mater. **12**, 1 (2024)

30. A. Chauhan, R. Verma, K.M. Batoo, S. Kumari, R. Kalia, R. Kumar, M. Hadi, E.H. Raslan, A. Imran, J. Mater. Res. **36**, 1496 (2021)
31. M. Farhadian, P. Sangpour, G. Hosseinzadeh, J. Energy Chem. **24**(2), 171 (2015)
32. Y. Yang, D. Xu, Q. Wu, P. Diao, Sci. Rep. **6**, 3515855 (2016)
33. B.H. Sun, H.F. Li, Q. Wei, S. Xue, A.J. Zhou, X.P. Yue, Sep. Purif. Technol. **301**, 122039 (2022)
34. A.A. Sakib, S.M. Masum, J. Hoinkis, R. Islam, M.A. Molla, J. Compos. Sci. **3**(3), 91 (2019)
35. H.J. Gao, H. Yang, S.F. Wang, Optik **175**, 237 (2018)
36. S. Gadge, A. Tamboli, M. Shinde, H. Fouad, C. Terashima, R. Chauhan, S. Gosavi, J. Solid State Electrochem. **27**(8), 2005 (2023)
37. N.B. Bokhale, S.D. Bomble, R.R. Dalbhanjan, D.D. Mahale, S.P. Hinge, B.S. Banerjee, A.V. Mohod, P.R. Gogate, Ultrason. Sonochem. **21**(5), 1797 (2014)
38. M. Kumar, M.N. Ansari, I. Boukhris, M.S. Al-Buriahi, Z.A. Alrowaili, N. Alfryyan, P. Thomas, R. Vaish, Glob. Chall. **6**(6), 2100132 (2022)
39. R.A. Shathy, S.A. Fahim, M. Sarker, M.S. Quddus, M. Moniruzzaman, S.M. Masum, M.A. Molla, Catalysts **12**(3), 308 (2022)

Authors and Affiliations

Hafize Nagehan Koysuren[1] · Ozcan Koysuren[2]

✉ Ozcan Koysuren
koysuren@ankara.edu.tr

Hafize Nagehan Koysuren
nagehan.koysuren@ahievran.edu.tr

[1] Department of Environmental Engineering, Kirsehir Ahi Evran University, 40100 Kirsehir, Türkiye

[2] Department of Energy Systems Engineering, Ankara University, 06830 Ankara, Türkiye